A Linear Response, DFT+U Study of Trends in the Oxygen Evolution Activity of Transition Metal Rutile Dioxides

Zhongnan Xu,[†] Jan Rossmeisl,[‡] and John R. Kitchin[∗,†]

Department of Chemical Engineering, Carnegie Mellon University, 5000 Forbes Ave, Pittsburgh, PA 15213, and Center for Atomic-Scale Materials Design, Department of Physics, Technical University of Denmark, Building 307, 2800 Kgs. Lyngby, Denmark

E-mail: jkitchin@andrew.cmu.edu

[∗]To whom correspondence should be addressed

[†]Department of Chemical Engineering, Carnegie Mellon University, 5000 Forbes Ave, Pittsburgh, PA 15213

[‡]Center for Atomic-Scale Materials Design, Department of Physics, Technical University of Denmark, Building 307, 2800 Kgs. Lyngby, Denmark

Abstract

There are known errors in oxidation energies of transition metal oxides caused by an improper treatment of their d-electrons. The Hubbard U is the computationally cheapest addition one can use to capture correct reaction energies, but the specific Hubbard U oftentimes must be empirically determined only when suitable experimental data exists. We evaluated the effect of adding a calculated, linear response U on the predicted adsorption energies, scaling relationships, and activity trends with respect to the oxygen evolution reaction for a set of transition metal dioxides. We find that applying a U greater than zero always causes adsorption energies to be more endothermic. Furthermore, the addition of the Hubbard U greater than zero does not break scaling relationships established without the Hubbard U. The addition of the calculated linear response U value produces shifts of different systems along the activity volcano that results in improved activity trends when compared with experimental results.

Keywords: density functional theory, oxygen evolution, scaling relationships, linear response U

Introduction

Density functional theory (DFT) is a first principles tool that can be used to understand catalytic processes and identify promising candidates through the calculation of kinetic and thermodynamic properties, which include formation energies, adsorption energies, and reaction barriers.[1–4] Transition metal oxides (TMOs), a class of catalysts used in a wide variety of important chemical processes,[5–7] have thermodynamic and electronic properties that are difficult to capture accurately using standard exchange correlation functionals (LDA and GGA).[8] The culprit of these inaccuracies is the self-interaction error produced by highly correlated electrons, such as the d-electrons in oxidized systems.[9,10] The Hubbard U (DFT+U) is the most feasible correction to account for the self-interaction error,[11,12] but its method

of application is not trivial. The specific Hubbard U required for a given material can be empirically determined, but the experimental data required oftentimes is not available. For example, adsorption energies on well defined surfaces of oxides are typically difficult to measure.[13] Bulk oxidation energies can be used, but the Hubbard U values are typically reaction specific.[9,14] In contrast, the Hubbard U can also be calculated via a linear response method,[15] but there have been few studies that use this method in for the calculation of catalytic properties.

One of the most studied reactions catalyzed by transition metal oxides is the oxygen evolution reaction.[16,17] The oxygen evolution reaction (OER) is the conversion of H_2O into protons, electrons and oxygen. The high energy of protons and electrons can be stored into the chemical bonds of hydrogen, alcohols, or hydrocarbons, while pure oxygen is a widely used oxidant in chemical industries and must be separated from N_2 if acquired from air. The observed trends in kinetics of OER on different catalysts can be related to calculated chemical and electronic properties transition metal oxides.[18–21] Key conclusions from these studies are that the adsorption energies of a few intermediates describe the activity trends, these adsorption energies scale with each other, and the scaling of adsorption energies produces an activity volcano with a theoretical activity limit. These conclusions were established without the Hubbard U. While a few studies have applied the Hubbard U to test cases,[22,23] it is still not clear whether the aforementioned conclusions still apply to with the application of the Hubbard U nor if the linear response U will lead to better agreement with experimental results.

In this study, we use DFT+U coupled with the calculated linear response U to evaluate trends in activity of transition metal rutile dioxides for the oxygen evolution reaction. We apply an atomistic thermodynamic method that relates the activity of surfaces to differences in the adsorption energies OH, O, and OOH. We find that the application of any U in almost all cases leads to more endothermic adsorption energies of all intermediates and these shifts in adsorption energies preserve the scaling relationships between OER intermediates calculated

with $U = 0$. The combination of both observations results in relatively small shifts of all systems to the weak binding side of the OER volcano. We find that these shifts leads to activity trends that are more consistent with experimental observations.

Methods

DFT calculation parameters

All DFT calculations were performed with QUANTUM-ESPRESSO[24] with the Perdew-Burke-Ernzerhof (PBE) exchange correlation functional.[25,26] The core electrons were described by the GBRV library of ultrasoft pseudopotentials.[27] The kinetic energy cutoff for wavefunctions and the charge density were 40 and 500 Ry, respectively. For surface slabs, we used a $4 \times 4 \times 1$ Monkhorst-Pack grid of k-points.[28] All calculations were spin-polarized.

The general method for the calculation of the linear response U is described in a previous paper by Cococcioni and de Gironcoli.[15] For calculation of linear response U values in the bulk, we applied perturbations up to ± 0.15 eV to both the metal and oxygen in $2 \times 2 \times 2$ rutile supercells consisting of 48 atoms to ensure that interactions between the perturbations were and their periodic images were minimal.
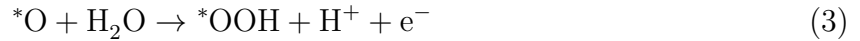
Structural parameters

The equilibrium volume, cell shape, atomic positions of all transition metal dioxide rutile structures were determined by constructing a polynomial equation of state and full relaxation of the shape and atomic coordinates. Ground state magnetic configurations were calculated for all materials, taking into consideration non-magnetic, ferromagnetic, and anti-ferromagnetic orderings.

All adsorption energies were performed on the (110) surface. Because of the large number of calculations we performed in this study, we chose to model the (110) surface as a two layer slab with terminating hydrogen atoms on the bottom layer. A similar two layer slab has

been used in previous studies of oxygen evolution on MnO_2 and IrO_2 surfaces.[29,30] The validation of this smaller slab with respect to the typical four layer slab used in similar previous studies[18,19,31] is discussed in the results. Figure 1 shows the two layer slab and four layer slab used for validation along with the adsorption site used for all calculations, which is typically called the 5*cus* site.

Atomistic thermodynamic framework for oxygen evolution

The atomistic thermodynamic framework we are using to study the oxygen evolution reaction has been used before,[18,19,32,33] so we only briefly summarize it below. The mechanism of OER is assumed to proceed through four electron proton transfer steps and the OH, O, and OOH intermediates, shown below in acidic conditions.

$$H_2O + * \rightarrow {}^*OH + H^+ + e^- \tag{1}$$

$$^*OH \rightarrow {}^*O + H^+ + e^- \tag{2}$$

$$^*O + H_2O \rightarrow {}^*OOH + H^+ + e^- \tag{3}$$

$$^*OOH \rightarrow * + O_2 + H^+ + e^- \tag{4}$$

At constant pH and with respect to the normal hydrogen electrode (NHE), the Gibbs free energy of each elementary step is shown below,

$$\Delta G_1 = \Delta G_{OH} \tag{5}$$

$$\Delta G_2 = \Delta G_O - \Delta G_{OH} \tag{6}$$

$$\Delta G_3 = \Delta G_{OOH} - \Delta G_O \tag{7}$$

$$\Delta G_4 = 4.92[eV] - \Delta G_{OOH} \tag{8}$$

where the adsorption energy of OH, O, and OOH are as follows

$$\Delta G_{\mathrm{O}} = E_{slab,\mathrm{O}} - E_{slab} - (E_{\mathrm{H_2O}} - E_{\mathrm{H_2}}) \tag{9}$$

$$\Delta G_{\mathrm{OH}} = E_{slab,\mathrm{OH}} - E_{slab} - (E_{\mathrm{H_2O}} - \frac{1}{2}E_{\mathrm{H_2}}) \tag{10}$$

$$\Delta G_{\mathrm{OOH}} = E_{slab,\mathrm{OH}} - E_{slab} - (2E_{\mathrm{H_2O}} - \frac{3}{2}E_{\mathrm{H_2}}) \tag{11}$$

where $E_{slab,A}$ is the total energy of slab with adsorbate A, E_{slab} is the total energy of the bare slab, and $E_{\mathrm{H_2O}}$ and $E_{\mathrm{H_2}}$ is the total energy of H_2O and H_2 in an asymmetric box. All adsorbate and gas species included previously reported zero point energy corrections.[19]

Because each reaction step involves the transfer of an electron to the electrode, applying a potential of U volts on the electrode with respect to NHE would result in a decrease of the ΔG of each reaction step by U eV. When a potential is applied such that the ΔG for all reaction steps is less than zero, all reaction steps are considered exothermic. The potential at which this happens minus 1.23 V is considered the theoretical overpotential, η^{OER}, and is the key metric we use to evaluate the activity of different catalysts for OER. The expression for η^{OER} is shown below in Equation (12),

$$\eta^{OER} = \mathrm{Max}[\Delta G_1, \Delta G_2, \Delta G_3, \Delta G_4]/e - 1.23V. \tag{12}$$

The existence of scaling relationships between different reaction energies ΔG gives rise to a descriptor and activity volcano where either ΔG_2 or ΔG_3 is the largest reaction energy and both of their magnitudes scale with the difference between the adsorption energies of O and OH ($\Delta G_O - \Delta G_{OH}$). The details of this analysis can be found in the seminal work that originally established this atomistic thermodynamics,[18,19] but we will be using this relationship to establish a similar volcano plot in our analysis.

Results and Discussion

Validation of the surface slab model

The TMOs we investigated are shown in Table 1 along with their equilibrium lattice constants, magnetic structure, and calculated linear response U. The lattice coordinates and magnetic structure were then used to construct the two and four layer slabs, which are shown in Figure 1 (a), while the linear response U was used when assessing the OER activity trends of the different oxides.

Table 1: **Table of transition metal dioxides we studied along with their corresponding equilibrium lattice parameters and magnetic configurations. *NM* and *FM* stand for nonmagnetic and ferromagnetic, respectively.**

Compound	a	c	u	Magnetic Structure	Linear response U
TiO_2	4.65	2.97	0.31	*NM*	4.95
CrO_2	4.38	2.90	0.30	*FM*	7.15
MnO_2	4.36	2.84	0.30	*FM*	6.63
NbO_2	4.94	2.96	0.29	*NM*	3.32
MoO_2	4.95	2.73	0.28	*NM*	4.83
RuO_2	4.53	3.18	0.31	*NM*	6.73
RhO_2	4.55	3.11	0.31	*NM*	5.97
ReO_2	4.95	2.68	0.28	*NM*	5.27
IrO_2	4.54	3.18	0.31	*NM*	5.91
PtO_2	4.59	3.23	0.31	*NM*	6.25

We first validate the usage of the two layer surface model shown in Figure 1 (a). We motivate the usage of this slab because we are performing over 400 calculations using U values and would like to minimize the computational cost. We first calculate the adsorption energies of OH, O, and OOH on both the two layer and four layer slab at $U = 0$ for all systems. Figure 1 (b) shows a parity plot between adsorption energies calculated on both slabs, and we see excellent agreement for OOH, good agreement for OH, and reasonable agreement for O. More importantly, Figure 1 (c) also shows that both sets of adsorption energies fall on the same scaling relationship. This suggests that a majority of the differences between the two adsorption energies are systematic, and that the underlying physics that results in the

scaling relationships is the same for both the two and four layer slab. Following these results, we moved on to calculate adsorption energies on the two layer slab at $U > 0$.
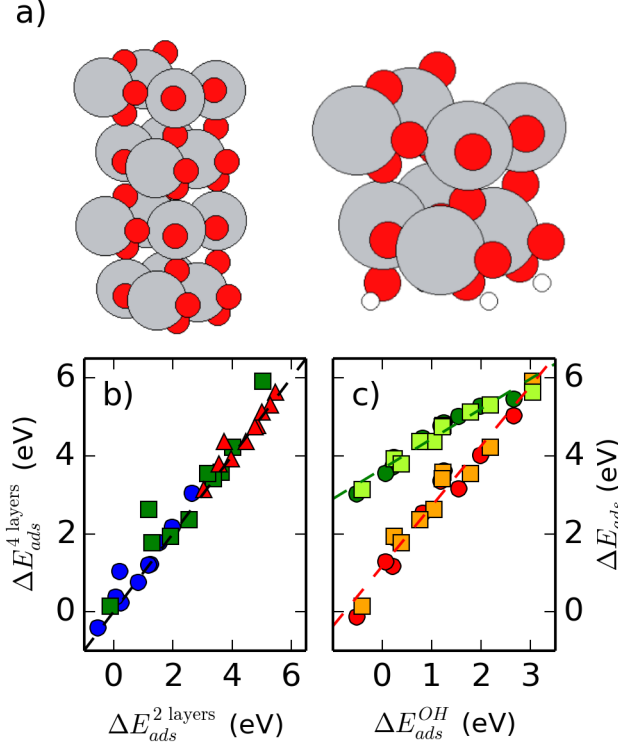

Figure 1: (a) The four layer rutile (110) surface (left) we used to validate the usage of the two slab (right) for DFT+U calculations of adsorption energies. (b) A parity plot between the adsorption energies of OH (blue circles), O (green squares), and OOH (red triangles) calculated at $U = 0$ on the two layer slab (x-axis) and four layer slab (y-axis). (c) Scaling relationships between of the adsorption energies of OH/O (orange markers) and OOH/OH (green markers) calculated with both the two layer slab (circles) and four layer slab (squares).

Variation of adsorption energies and scaling relationships with respect to U

For all materials, we calculated the adsorption energies by applying a $U = 0$ eV to $U = 8$ eV in 0.5 eV intervals. The starting geometry was taken from the relaxed structure of the calculation at $U = 0$. The entirety of our results can be found in the supporting information,[34] but for brevity we discuss results for only NbO_2, IrO_2, TiO_2, and MnO_2 below. Observations for NbO_2 and IrO_2 were characteristic of early and late $4d$ and $5d$ transition

metal dioxides, respectively. For $3d$ systems, TiO_2 is a special case, and observations for MnO_2 and CrO_2 were similar.
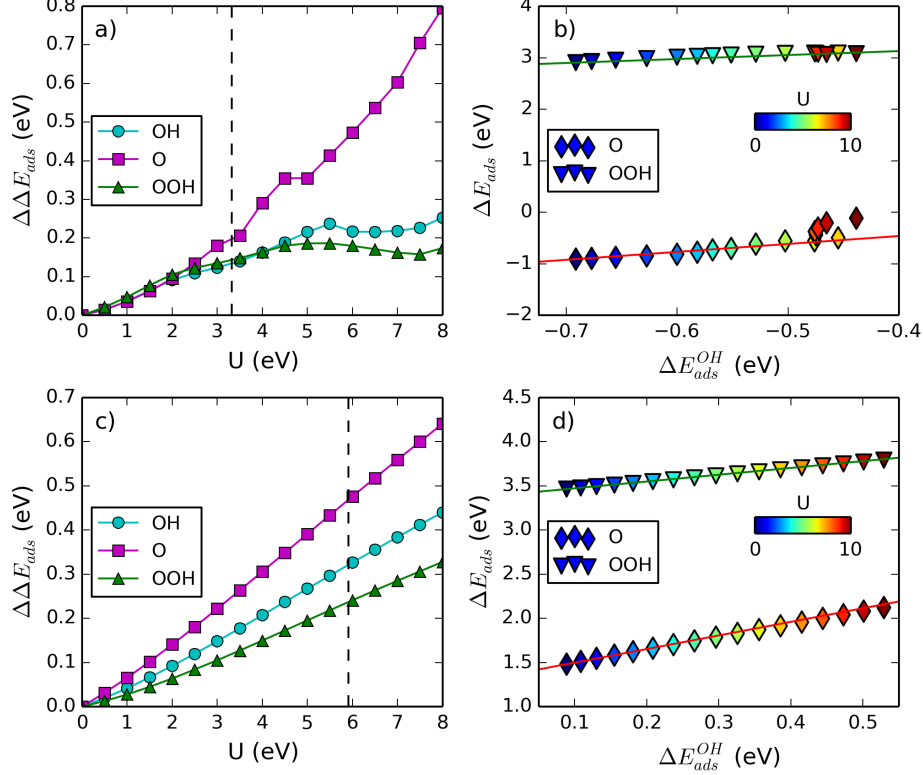

Figure 2: (a) and (c) show the dependence of the adsorption energies of OH, O, and OOH on U on NbO_2 and IrO_2, while (b) and (d) show the effect of U on the OH/O and OH/OOH scaling relationships on NbO_2 and IrO_2. In (a) and (c), the vertical dashed line shows the value of the linear response U value for the bulk oxide. In (b) and (d), the applied value of the U is shown by the color of the marker. The scaling relationships calculated at $U = 0$, shown in Figure 1 (c), are reproduced in (b) and (d) for the OH/O (red line) and OH/OOH (green line) offset to the adsorption energy at $U = 0$ of the particular compound for clarity.

We found that the application of $U > 0$ had a number of systematic effects to the adsorption energies of OH, O, and OOH to the $4d$ and $5d$ TMO rutiles. These are summarized in Figure 2. First, the application of U results in shifts to more endothermic adsorption energies of all species on all compounds (Figure 2 (a) and (c)). For low U values, these shifts are monotonic and smooth, but for high U values on early TMOs of MoO_2, NbO_2, and ReO_2, they deviate from the monotonic trend at low U values. It is likely that such high values of U are not appropriate for these early TMOs. Early TMOs have a smaller

9

occupancy of d-electrons, and therefore one would expect a lower value of U is needed to correct the self-interaction error. This is supported by the lower linear response U for the early $4d$ and $5d$ TMOs (Table 1). We also observed that the calculated linear response U for all early $4d$ and $5d$ TMOs sits right at the point where the smooth, monotonic $\Delta E_{ads}(U)$ behavior breaks down. This is shown for NbO_2 in Figure 2 (a) and the rest of the early TMOs in the supporting information. This is further evidence that high U values are not appropriate for early TMOs. For late TMOs of PtO_2, IrO_2, RuO_2, and RhO_2, the changes are smooth all the way up to a $U = 8$, including their calculated linear response U values.

For $4d$ and $5d$ oxides, the U-induced endothermic changes of the adsorption energy preserve scaling relationships established at $U = 0$. This is shown in Figure 2 (b) and (d). This is true for all U values tested on the $4d$ and $5d$ TMOs, including high U values on early TMOs. Our results further demonstrates the robustness of scaling relationships, showing that the additional physics via the Hubbard U does not lead to deviations of scaling relationships. This also demonstrates that correlations between the electronic structure and adsorption energies implied by the scaling relationships are also preserved with the addition of U. This conclusion is consistent with previous work that found similar electronic structure/activity correlations on doped TiO_2 with both DFT and DFT+U results.[35]
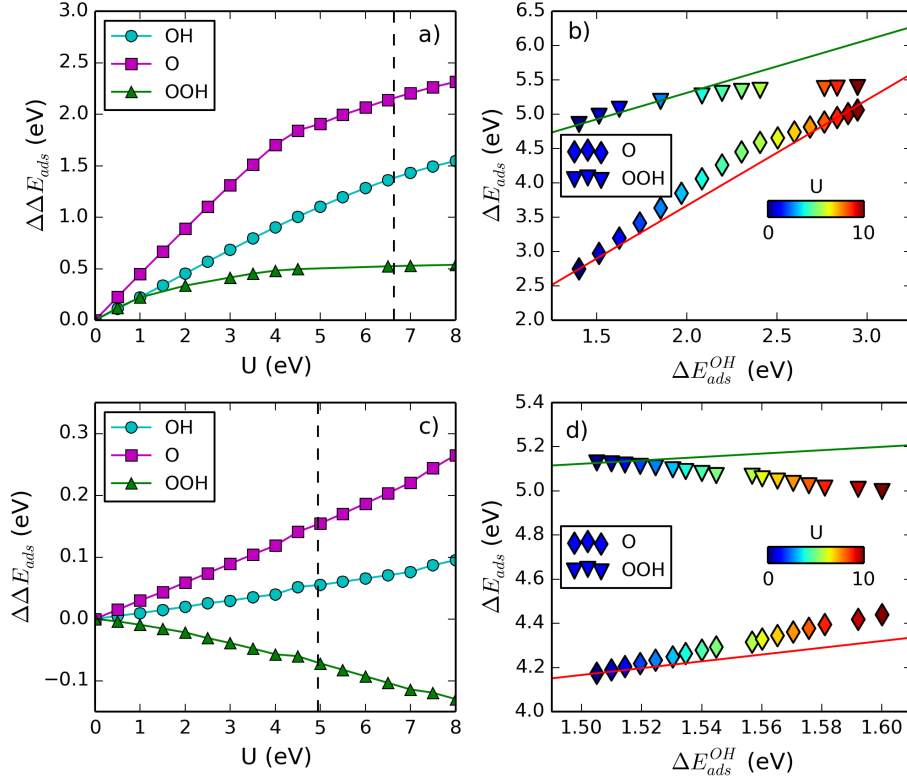
Figure 3: (a) and (c) show the dependence of the adsorption energies of OH, O, and OOH on U on MnO_2 and TiO_2, while (b) and (d) show the effect of U on the OH/O and OH/OOH scaling relationships on MnO_2 and TiO_2. In (a) and (c), the verticle dashed line shows the value of the linear response, calculated U value for the bulk oxide. In (b) and (d), the applied value of the U is shown by the color of the marker. The scaling relationships calculated at $U = 0$, shown in Figure 1 (c), are reproduced in (b) and (d) for the OH/O (red line) and OH/OOH (green line) offset to the adsorption energy at $U = 0$ of the particular compound for clarity.

In contrast to our results on 4d and 5d TMOs, we found a mixture of results for 3d TMOs. Adsorption energies at $U > 0$ on CrO_2 and MnO_2 gave similar results to each other, with adsorption on MnO_2 shown in Figure 3 (a) and (b). With increasing U values, we observe a smooth monotonic increase in the adsorption energy, but at some intermediate U value adsorption of OOH on the surface is no longer stable for some species, shown by the lack of change in adsorption energy for $U > 4$ eV for MnO_2. This is what gives rise to the breaking of the scaling relationship between OH and OOH at $U \approx 4$ eV. We are unsure how to interpret the breaking of the surface-adsorbate bonds, but it is clear that even at low U

11

values when adsorption was stable, the scaling relationships are preserved. This is consistent with our results on $4d$ and $5d$ TMO rutiles.

For TiO_2, application of U produces smooth, monotonic changes in the adsorption energy (Figure 3 (c)), but interestingly the change in the OOH adsorption energy is exothermic upon increasing U. This was the only adsorption energy where the addition of U produced a more exothermic adsorption energy. Also unique to TiO_2 is that the scaling relationships are not preserved with the addition of U (Figure 3 (d)). The relative change in the adsorption energy with respect to increasing U is also small. ΔE_{ads}^{OH} changes by less than 0.1 eV by applying a U value of 8 eV.

There is still conflicting literature on how the Hubbard U should be implemented to capture accurate thermodynamic properties of Ti oxide systems.[14,36–38] Our results show this is still an open issue for adsorption on TiO_2. The Ti ion at the adsorption site of a stoichiometric TiO_2 has a d^0 configuration and OH, O, or OOH primarily forms bonds with the $3p$ electrons. Hence, adsorption induced changes to the electronic structure of the Ti d electrons are subtle, which is reflected by the smaller change in the adsorption energies induced by adding a Hubbard U. This electronic structure phenomenon is typical for stoichiometric surfaces of closed shell materials, such as adsorption on stoichiometric alkaline-earth metal oxides,[39] and leads to deviations in trends of both adsorption and oxygen vacancy formation energies with respect to number of electrons.[40–42] This situation is not encountered in any other of the adsorption eneriges we studied.

Because of this unique change in the electronic structure caused by adsorption on TiO_2, we hypothesize that the application of the Hubbard U to the d-electrons of the TiO_2 after adsorption may require different treatment. The U we calculated for bulk TiO_2 likely does not describe the TiO_2 with a $3p$ hole state. To resolve this special case, one might be required to calculate separate Hubbard U values of the Ti ion with and without an adsorbate and use the DFT+U(R) method to calculate an adsorption energy that takes changes in U into account.[43] Another possibility is the requirement of application of U to lattice oxygen $2p$

states or Ti $3p$ states. A relatively high U of 6 eV applied to the oxygen $2p$ states was required to accurately capture hole states in SiO_2 doped with Al.[44]

To summarize, we draw two main conclusions from our analysis of adsorption energies and scaling relationships with respect to increasing U values. With the exception of TiO_2, where the significance of the Hubbard U to calculate adsorption on TiO_2 remains unclear, the application of U produces more endothermic adsorption energies, and these changes in adsorption energy preserve the scaling relationships established at $U = 0$. These conclusions further validate the scaling relationships and their usage for establishing models for catalytic reactions on TMOs.[45] The similar weakening of adsorption energies with respect to U also suggests that a majority of trend studies of adsorption on TMOs at $U = 0$ are probably valid at $U > 0$. Our results also provide researchers with useful estimates on the effect of U on adsorption energies. Having established some general rules between the Hubbard U, adsorption energies, and scaling relationships, we now move towards the specific application of OER and the usage of the linear response calculated U.

Activity trends with linear response U value

We next evaluate the effect of applying a calculated linear response Hubbard U to the activity trends for OER. We focus our analysis on the IrO_2, PtO_2, RuO_2, and RhO_2 oxides in our study. We choose only these materials for a number of reasons. First, from Pourbaix diagrams, one can easily see that CrO_2, MoO_2, NbO_2 and ReO_2 are not stable in either acidic or alkaline OER conditions.[46] In contrast, IrO_2, PtO_2, RuO_2, and RhO_2 are predicted to be stable at acidic OER conditions and in some cases have been observed *in situ* in experimental work.[46–48] MnO_2 was not used in this comparison for two reasons. First, it is still unclear whether MnO_2 is the active species at OER conditions. Recent studies have identified that the Mn^{3+} as the active species in OER.[49,50] Second, our results point towards OOH desorption at the linear response, calculated U value. TiO_2 was not used in our comparison due to our conclusion that our DFT+U method did not seem appropriate for

13

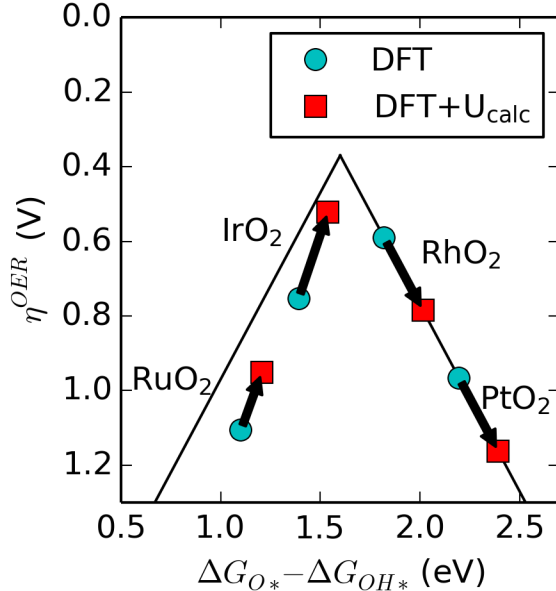an accurate calculation of adsorption energies and it is not a good OER catalyst.

Figure 4: The predicted activity trends of 4d and 5d rutile dioxides calculated without (blue circle) and with (red square) the linear response U. Arrow points in the effect of applying the linear response U. The volcano is fit to the idealized scaling relationships determined in a previous paper.[19]

Figure 4 shows the changes in the activity of the selected oxides as one applies the linear response, calculated Hubbard U. As expected from the observed preservation of scaling relationships, the changes in the adsorption energy produced by applying the linear response U for all species results in movement along the weak binding and strong binding legs of the volcano, but *not* changes in the activity volcano itself. Furthermore, all species are moved towards the weaker binding leg of the volcano, which is explained by the universal weakening of adsorption energies caused by applying the Hubbard U.

The combination of these two observations leads to changes in the relative ordering of activity. With DFT, we predict the activity trend to be $RhO_2 > IrO_2 > PtO_2 > RuO_2$. With the addition of the calculated Hubbard U, we now predict the activity to be $IrO_2 > RhO_2 > RuO_2 > PtO_2$. The ordering with the addition of the Hubbard U shows better agreement with experiments, which has been observed as $RuO_2 \approx IrO_2 > RhO_2 > PtO_2$.[51,52]

14

We still obtain discrepancy with regard to the activity of RuO_2 with respect to RhO_2, but the addition of U improves agreement with experimentally observed trends. IrO_2 and RuO_2 move towards the top of the volcano from the strong binding side, while RhO_2 and PtO_2 move away from the top of the volcano on the weak binding side. The combination of these two effects corrects the incorrect ordering of $RhO_2 > IrO_2$ and $PtO_2 > RuO_2$. We note that previous results observed a different ordering between these compounds, found to be $RuO_2 > PtO_2 \approx RhO_2 > IrO_2$, at $U = 0$. We associate these slight differences with differences in pseudopotentials, calculation parameters, and the implementation of different surface models. However, both set of results saw IrO_2 and RuO_2 on the strong binding (left) side of the volcano and RhO_2 and PtO_2 on the weak binding (right) side of the volcano. Hence, it is likely the application of the linear response U to those results should give similar improvements to those seen here, with IrO_2 predicted to be more active than PtO_2 and RhO_2.

We also comment that though changes in ordering are observed, the absolute changes in reaction energies are relatively small. The changes in reaction energy with the application of the calculated U value was on the order of $0.2 \sim 0.4$ eV, which in no case was enough to move a species from the strong binding to weak binding side of the volcano. Hence, we propose that large scale screening studies based on correlations between adsorption energies done without and with the Hubbard U should produce similar conclusions, except perhaps near the top of the volcano.

Conclusions

To summarize, we have performed a DFT$+U$ study on the adsorption of OER intermediates on the (110) surface of rutile transition metal dioxides. Our analysis focused on changes in the adsorption energy, scaling relationships, and activity trends by applying a range of Hubbard U values in addition to the linear response, calculated U value. We find that with

the exception of TiO_2, the application of a large range of Hubbard U values produces more endothermic adsorption energies and preserves scaling relationships established at $U = 0$. We also find that when linear response U values applied, the relative ordering of the activity of IrO_2, PtO_2, RuO_2, and RhO_2 oxides improves with respect to experimental observations. Our work reveals a number of universal relationships between the Hubbard U and catalytic processes on transition metal oxides.

Acknowledgement

Supporting Information Available

Full details of the computational setup and analysis of the computations is available. All input and output files can be found online at http://dx.doi.org/10.5281/zenodo.12635, and the supporting information contains scripts used for generating and analyzing these files. This material is available free of charge via the Internet at `http://pubs.acs.org/`.

References

(1) Nørskov, J. K.; Bligaard, T.; Rossmeisl, J.; Christensen, C. H. Towards the Computational Design of Solid Catalysts. *Nat. Chem.* **2009**, *1*, 37–46.

(2) Greeley, J.; Jaramillo, T. F.; Bonde, J.; Chorkendorff, I. B.; Nørskov, J. K. Computational High-throughput Screening of Electrocatalytic Materials for Hydrogen Evolution. *Nat. Mater.* **2006**, *5*, 909–913.

(3) Nørskov, J. K.; Bligaard, T.; Logadottir, A.; Bahn, S.; Hansen, L.; Bollinger, M.;

Bengaard, H.; Hammer, B.; Sljivancanin, Z.; Mavrikakis, M. et al. Universality in Heterogeneous Catalysis. *J. Catal.* **2002**, *209*, 275–278.

(4) Michaelides, A.; Liu, Z.-P.; Zhang, C. J.; Alavi, A.; King, D. A.; Hu, P. Identification of General Linear Relationships Between Activation Energies and Enthalpy Changes for Dissociation Reactions At Surfaces. *J. Am. Chem. Soc.* **2003**, *125*, 3704–3705.

(5) Weaver, J. F. Surface Chemistry of Late Transition Metal Oxides. *Chem. Rev.* **2013**, *113*, 4164–4215.

(6) Doyle, R. L.; Godwin, I. J.; Brandon, M. P.; Lyons, M. E. G. Redox and Electrochemical Water Splitting Catalytic Properties of Hydrated Metal Oxide Modified Electrodes. *Phys. Chem. Chem. Phys.* **2013**, *15*, 13737–13783.

(7) Gouma, P. Nanoscale Polymorphic Oxides for Selective Chemosensors. *Sci. Adv. Mater.* **2011**, *3*, 787–793.

(8) Cohen, A. J.; Mori-Sánchez, P.; Yang, W. Insights into Current Limitations of Density Functional Theory. *Science* **2008**, *321*, 792–794.

(9) Wang, L.; Maxisch, T.; Ceder, G. Oxidation Energies of Transition Metal Oxides Within the GGA + U Framework. *Phys. Rev. B* **2006**, *73*, 195107.

(10) Franchini, C.; Podloucky, R.; Paier, J.; Marsman, M.; Kresse, G. Ground-State Properties of Multivalent Manganese Oxides: Density Functional and Hybrid Density Functional Calculations. *Phys. Rev. B* **2007**, *75*, 195128.

(11) Anisimov, V. I.; Aryasetiawan, F.; Lichtenstein, A. First-principles Calculations of the Electronic Structure and Spectra of Strongly Correlated Systems: the LDA + U Method. *J. Phys. Condens. Matter* **1997**, *9*, 767.

(12) Anisimov, V. I.; Zaanen, J.; Andersen, O. K. Band Theory and Mott Insulators: Hubbard U Instead of Stoner I. *Phys. Rev. B* **1991**, *44*, 943.

(13) Campbell, C. T.; Sellers, J. R. V. Enthalpies and Entropies of Adsorption on Well-Defined Oxide Surfaces: Experimental Measurements. *Chem. Rev.* **2013**, *113*, 4106–4135.

(14) Aykol, M.; Wolverton, C. Local Environment Dependent GGA+ U Method for Accurate Thermochemistry of Transition Metal Compounds. *Phys. Rev. B* **2014**, *90*, 115105.

(15) Cococcioni, M.; de Gironcoli, S. Linear Response Approach To the Calculation of the Effective Interaction Parameters in the LDA + U Method. *Phys. Rev. B* **2005**, *71*, 035105.

(16) Dau, H.; Limberg, C.; Reier, T.; Risch, M.; Roggan, S.; Strasser, P. The Mechanism of Water Oxidation: From Electrolysis Via Homogeneous To Biological Catalysis. *ChemCatChem* **2010**, *2*, 724–761.

(17) Parent, A. R.; Sakai, K. Progress in Base-Metal Water Oxidation Catalysis. *ChemSusChem* **2014**, *7*, 2070–2080.

(18) Rossmeisl, J.; Qu, Z.-W.; Zhu, H.; Kroes, G.-J.; Nørskov, J. K. Electrolysis of Water on Oxide Surfaces. *J. Electroanal. Chem.* **2007**, *607*, 83–89.

(19) Man, I. C.; Su, H.-Y.; Calle-Vallejo, F.; Hansen, H. A.; Martínez, J. I.; Inoglu, N. G.; Kitchin, J.; Jaramillo, T. F.; Nørskov, J. K.; Rossmeisl, J. Universality in Oxygen Evolution Electrocatalysis on Oxide Surfaces. *ChemCatChem* **2011**, *3*, 1159–1165.

(20) Suntivich, J.; May, K. J.; Gasteiger, H. A.; Goodenough, J. B.; Shao-Horn, Y. A Perovskite Oxide Optimized for Oxygen Evolution Catalysis From Molecular Orbital Principles. *Science* **2011**, *334*, 1383–1385.

(21) Vojvodic, A.; Norskov, J. K. Optimizing Perovskites for the Water-splitting Reaction. *Science* **2011**, *334*, 1355–1356.

(22) Liao, P.; Keith, J. A.; Carter, E. A. Water Oxidation on Pure and Doped Hematite (0001) Surfaces: Prediction of Co and Ni As Effective Dopants for Electrocatalysis. *J. Am. Chem. Soc.* **2012**, *134*, 13296–13309.

(23) Garcia-Mota, M.; Bajdich, M.; Viswanathan, V.; Vojvodic, A.; Bell, A. T.; Nørskov, J. K. Importance of Correlation in Determining Electrocatalytic Oxygen Evolution Activity on Cobalt Oxides. *J. Phys. Chem. C* **2012**, *116*, 21077–21082.

(24) Giannozzi, P.; Baroni, S.; Bonini, N.; Calandra, M.; Car, R.; Cavazzoni, C.; Ceresoli, D.; Chiarotti, G. L.; Cococcioni, M.; Dabo, I. et al. Quantum ESPRESSO: a modular and open-source software project for quantum simulations of materials. *Journal of Physics: Condensed Matter* **2009**, *21*, 395502.

(25) Perdew, J. P.; Burke, K.; Ernzerhof, M. Generalized Gradient Approximation Made Simple. *Phys. Rev. Lett.* **1996**, *77*, 3865–3868.

(26) Perdew, J. P.; Burke, K.; Ernzerhof, M. Generalized Gradient Approximation Made Simple. *Phys. Rev. Lett.* **1997**, *78*, 1396–1396.

(27) Garrity, K. F.; Bennett, J. W.; Rabe, K. M.; Vanderbilt, D. Pseudopotentials For High-Throughput DFT Calculations. *Comp. Mater. Sci* **2014**, *81*, 446–452.

(28) Monkhorst, H. J.; Pack, J. D. Special Points for Brillouin-Zone Integrations. *Phys. Rev. B* **1976**, *13*, 5188–5192.

(29) Steegstra, P.; Busch, M.; Panas, I.; Ahlberg, E. Revisiting the Redox Properties of Hydrous Iridium Oxide Films in the Context of Oxygen Evolution. *J. Phys. Chem. C* **2013**, *117*, 20975–20981.

(30) Busch, M.; Ahlberg, E.; Panas, I. Water Oxidation on MnO_x and IrO_x: Why Similar Performance? *J. Phys. Chem. C* **2012**, *117*, 288–292.

(31) Halck, N. B.; Petrykin, V.; Krtil, P.; Rossmeisl, J. Beyond the Volcano Limitations in Electrocatalysis - Oxygen Evolution Reaction. *Phys. Chem. Chem. Phys.* **2014**, *16*, 13682–13688.

(32) Mom, R. V.; Cheng, J.; Koper, M. T. M.; Sprik, M. Modeling the Oxygen Evolution Reaction on Metal Oxides: The Infuence of Unrestricted DFT Calculations. *J. Phys. Chem. C* **2014**, *118*, 4095–4102.

(33) Calle-Vallejo, F.; Martínez, J.; García-Lastra, J. M.; Abad, E.; Koper, M. T. M. Oxygen Reduction and Evolution At Single-metal Active Sites: Comparison Between Functionalized Graphitic Materials and Protoporphyrins. *Surf. Sci.* **2013**, *607*, 47–53.

(34) Xu, Z.; Rossmeisl, J.; Kitchin, J. R. Supporting data for: A linear response, DFT+U study of trends in the oxygen evolution activity of transition metal rutile dioxides. doi:10.5281/zenodo.12635.

(35) García-Mota, M.; Vojvodic, A.; Abild-Pedersen, F.; Nørskov, J. K. Electronic Origin of the Surface Reactivity of Transition-Metal-Doped TiO_2 (110). *J. Phys. Chem. C* **2012**, *117*, 460–465.

(36) Jain, A.; Hautier, G.; Moore, C. J.; Ping Ong, S.; Fischer, C. C.; Mueller, T.; Persson, K. A.; Ceder, G. A High-throughput Infrastructure for Density Functional Theory Calculations. *Comp. Mater. Sci.* **2011**, *50*, 2295–2310.

(37) Hu, Z.; Metiu, H. Choice of U for DFT+U Calculations for Titanium Oxides. *J. Phys. Chem. C* **2011**, *115*, 5841–5845.

(38) Yan, J.; Nørskov, J. K. Calculated Formation and Reaction Energies of 3*d* Transition Metal Oxides Using a Hierarchy of Exchange-Correlation Functionals. *Phys. Rev. B* **2013**, *88*, 245204.

(39) Bajdich, M.; Nørskov, J. K.; Vojvodic, A. Surface Energetics of Alkaline-Earth Metal Oxides: Trends in Stability and Adsorption of Small Molecules. *arXiv preprint arXiv:1412.6585* **2014**,

(40) Akhade, S. A.; Kitchin, J. R. Effects of Strain, d-Band Filling, and Oxidation State on the Surface Electronic Structure and Reactivity of 3d Perovskite Surfaces. *J. Chem. Phys.* **2012**, *137*, 084703.

(41) Calle-Vallejo, F.; Inoglu, N. G.; Su, H.-Y.; Martinez, J. I.; Man, I. C.; Koper, M. T. M.; Kitchin, J. R.; Rossmeisl, J. Number of Outer Electrons As Descriptor for Adsorption Processes on Transition Metals and Their Oxides. *Chem. Sci.* **2013**, *4*, 1245–1249.

(42) Curnan, M. T.; Kitchin, J. R. Effects of Concentration, Crystal Structure, Magnetism, and Electronic Structure Method on First-Principles Oxygen Vacancy Formation Energy Trends in Perovskites. *J. Phys. Chem. C* **2014**, *118*, 28776–28790.

(43) Kulik, H. J.; Marzari, N. Accurate Potential Energy Surfaces With a DFT+U(R) Approach. *J. Chem. Phys.* **2011**, *135*, 194105–194105.

(44) Nolan, M.; Watson, G. W. Hole Localization in Al Doped Silica: A DFT+U Description. *J. Chem. Phys.* **2006**, *125*, 144701.

(45) Medford, A. J.; Wellendorff, J.; Vojvodic, A.; Studt, F.; Abild-Pedersen, F.; Jacobsen, K. W.; Bligaard, T.; Nørskov, J. K. Assessing the Reliability of Calculated Catalytic Ammonia Synthesis Rates. *Science* **2014**, *345*, 197–200.

(46) Pourbaix, M. Atlas of Electrochemical Equilibria in Aqueous Solutions. **1974**,

(47) Sanchez Casalongue, H. G.; Ng, M. L.; Kaya, S.; Friebel, D.; Ogasawara, H.; Nilsson, A. In Situ Observation of Surface Species on Iridium Oxide Nanoparticles during the Oxygen Evolution Reaction. *Angew. Chem. Int. Ed.* **2014**, *126*, 7297–7300.

21

(48) Silva, L. M. D.; Boodts, J. F. C.; DeFaria, L. A. 'In Situ' and 'Ex Situ' Characterization of the Surface Properties of the $RuO_2(x)+Co_3O_4(1-x)$ System. *Electrochim. Acta* **2000**, *45*, 2719–2727.

(49) Ramírez, A.; Hillebrand, P.; Stellmach, D.; May, M. M.; Bogdanoff, P.; Fiechter, S. Evaluation of MnO_x, Mn_2O_3, and Mn_3O_4 Electrodeposited Films for the Oxygen Evolution Reaction of Water. *J. Phys. Chem. C* **2014**, *118*, 14073–14081.

(50) Gorlin, Y.; Jaramillo, T. F. A Bifunctional Nonprecious Metal Catalyst for Oxygen Reduction and Water Oxidation. *J. Am. Chem. Soc.* **2010**, *132*, 13612–13614.

(51) Miles, M. H.; Thomason, M. A. Periodic Variations of Overvoltages for Water Electrolysis in Acid Solutions From Cyclic Voltammetric Studies. *J. Electrochem. Soc.* **1976**, *123*, 1459–1461.

(52) Cherevko, S.; Zeradjanin, A. R.; Topalov, A. A.; Kulyk, N.; Katsounaros, I.; Mayrhofer, K. J. Dissolution of Noble Metals During Oxygen Evolution in Acidic Media. *ChemCatChem* **2014**, *6*, 2219–2223.

Graphical TOC Entry

$2\,H_2O \rightarrow O_2 + 4\,H^+ + 4\,e^-$

η^{OER}

Hubbard U

$\Delta G_{O*} - \Delta G_{OH*}$